Dynamic GNSS Mission Planning Using DTM for Precise Navigation of Autonomous Vehicles

Aleksander Nowak

(*Gdansk University of Technology, Faculty of Civil and Environmental Engineering*)
(E-mail: aleksander.nowak@geodezja.pl)

Nowadays, the most widely used method for estimating location of autonomous vehicles in real time is the use of Global Navigation Satellite Systems (GNSS). However, positioning in urban environments using GNSS is hampered by poor satellite geometry due to signal obstruction created by both man-made and natural features of the urban environment. The presence of obstacles is the reason for the decreased number of observed satellites as well as uncertainty of GNSS positioning. It is possible that in some sections of the vehicle route there might not be enough satellites necessary to fix position. It is common to use software for static GNSS measurement campaign planning, but it is often only able to predict satellite visibility at one point. This article presents a proposal for dynamic GNSS mission planning using a Digital Terrain Model (DTM) and dead reckoning. The methodology and sample results of numerical experiments are also described. They clearly show that proper dynamic GNSS mission planning is necessary in order to complete a task by an autonomous vehicle in an obstructed environment.

KEYWORDS

1. GNSS availability.   2. GNSS mission planning.   3. Autonomous navigation.

1. INTRODUCTION. Cities are challenging environments for positioning using Global Navigation Satellite Systems (GNSS) (Dong et al., 2015; Angrisano et al, 2013; Suh and Shibasaki, 2007). At the time of writing (November 2015), there are two autonomous fully operational systems: American GPS (Global Positioning System) and Russian GLONASS (GLObal NAvigation Satellite System) supported by Satellite-Based Augmentation Systems (SBAS). The European autonomous system Galileo and the Chinese BeiDou are still under development and are gradually being deployed. In spite of high fix accuracy (Asavasuthirakul and Karimi, 2013), global coverage (Gibons et al., 2013) and low cost of receivers which can be easily integrated into other navigation systems and devices, the main shortcoming of GNSS is satellite signal blockage when a vehicle is operating within obstructed environments such as urban canyons (Karimi and Asavasuthirakul, 2014; Roongpboonsopit and Karimi, 2012; Taylor et al., 2007). In addition, range measurement to satellites is

severely degraded by multipath effect (Li et al., 2006). Buildings act as reflectors for satellite signals, resulting in pseudorange measurement errors (Bradbury et al., 2007). Multipath reflection is a separate problem not considered in this paper but widely described in many papers, for example in (Soloviev and Van Graas, 2009; Janowski et al., 2014; Nowak, 2015). Here, we focus on the problem of satellite signal blockage by man-made and natural features of the urban environment.

Although interoperation of GPS and GLONASS provides visibility of several satellites in the open air, among high buildings the number of observed satellites significantly decreases and they form poor geometry – Dilution Of Precision (DOP) coefficients increase and hence positioning accuracy decreases. This is described, for example in Nowak and Specht (2008) and Radisic et al. (2010). Sometimes the number of visible satellites is fewer than four and then positioning is unavailable. This is not a problem as long as the gaps between GNSS fixes do not last too long and navigation is supported by additional alternative positioning methods (Dah et al., 2013; Godha and Cannon, 2007; Grejner-Brzezinska et al., 2001; Kitamura et al., 2011). Nevertheless, if we talk about autonomous navigation of small unmanned vehicles, a high availability of GNSS appears to be crucial in order to complete the task. This problem is considered for example in Kitamura et al. (2013) and Karimi and Asavasuthirakul (2014) but usually in the context of how to select the optimal route for an autonomous robot. In some tasks the vehicle route is strictly determined because of (for example) the fact that a robot has to inspect pointed objects of interest or pick something up from the specified location. In such cases success of the mission depends directly on positioning accuracy.

The constellation of GNSS satellites changes all the time and as the results of the experiments show, distribution of positioning availability and fix accuracy are not the same throughout the day (Janowski et al., 2014). Therefore dynamic GNSS mission planning seems to be necessary. The proposed method of GNSS positioning availability computation using a Digital Terrain Model (DTM) and dead reckoning allows us to choose the best time to complete the task by a small autonomous vehicle operating in an urban environment.

2. GNSS POSITIONING ACCURACY OVERVIEW. The observed value in GNSS is range to satellite, measured on the basis of the difference between receiving and sending time of the navigation signal. Due to the fact that the value of the user's clock error is unknown the range is called pseudorange. The pseudorange measurement to a particular satellite can be described by the following observation equation (Parkinson and Spilker, 1996):

$$\rho_i = R_i + c \cdot \delta T + \varepsilon_i = \sqrt{(x_{si} - x_u)^2 + (y_{si} - y_u)^2 + (z_{si} - z_u)^2} + c \cdot \delta T + \varepsilon_i , \quad (1)$$

where ρ_i is the measured pseudorange to the *i-th* satellite, R_i is the geometrical range to the *i-th* satellite, c is the mean speed of signal propagation, δT is the user's clock error and ε_i is the random measurement error, which is a composition of errors connected with ephemerids uncertainty, satellite clock error, ionospheric and tropospheric refraction, and noises of the user's receiver. x_{si}, y_{si}, z_{si} are the *i-th* satellite position in the Earth-Centred Earth-Fixed (ECEF) coordinates system and x_u, y_u, z_u is the user position in the ECEF coordinate system.

Satellite position is known at the time of measurement, because it can be calculated on the basis of data in the navigation message transmitted by the satellite. If it is additionally assumed that random measurement error can be modelled as an independent variable with zero-mean Gaussian distribution (N[0,1]) then Equation (1) will have four unknowns: user coordinates (x_u, y_u, z_u) and value $(c \cdot \delta T)$ which is called metre equivalent of the user's receiver clock error. Therefore, pseudorange measurement to at least four satellites is necessary to fix the user's position. This is the first and fundamental condition of GNSS positioning availability. The second is connected with desired accuracy, which can be estimated as (Parkinson and Spilker, 1996):

$$M = \sigma_p \cdot DOP \tag{2}$$

where M is the user's position mean error, σ_p is the root mean square of pseudorange measurements, depending on random errors (ε). For typical code receivers it is on the level of single metres and DOP is the coefficient of Dilution of Precision, depending on the satellite geometry (satellites location in relation to the user's position).

DOP coefficients can be calculated on the basis of a geometric matrix. Equation (1) is non-linear and to solve it, linearization is necessary. Usually Taylor's method is applied which is based on *a priori* information about the user's location. After linearization, Equation (1) takes the following form:

$$\rho_i - R_{0i} = \frac{-(x_{si} - x_{0u})}{R_{0i}} \cdot \Delta x + \frac{-(y_{si} - y_{0u})}{R_{0i}} \cdot \Delta x + \frac{-(z_{si} - z_{0u})}{R_{0i}} \cdot \Delta z + c \cdot \delta T \tag{3}$$

where x_{0u}, y_{0u}, z_{0u} are the *a priori* assumed user coordinates, Δx, Δy, Δz are the differences between true and *a priori* assumed user coordinates and R_{0i} is geometrical range from the *a priori* assumed user coordinates to *i-th* satellite:

$$R_0 = \sqrt{(x_{si} - x_{0u})^2 + (y_{si} - y_{0u})^2 + (z_{si} - z_{0u})^2} \tag{4}$$

All observation Equations (3) which describe performed pseudorange measurements to *n* visible satellites create the following matrix equation system:

$$\begin{bmatrix} \rho_1 - R_{01} \\ \rho_2 - R_{02} \\ \vdots \\ \rho_n - R_{0n} \end{bmatrix} = \begin{bmatrix} -u_{x1} & -u_{y1} & -u_{z1} & 1 \\ -u_{x2} & -u_{y2} & -u_{z2} & 1 \\ & \vdots & & \\ -u_{xn} & -u_{yn} & -u_{zn} & 1 \end{bmatrix} \cdot \begin{bmatrix} \Delta x \\ \Delta y \\ \Delta z \\ c \cdot \delta T \end{bmatrix} \tag{5}$$

$$\Delta \boldsymbol{\rho} = \mathbf{G} \overset{\Downarrow}{\cdot} \Delta \mathbf{X}, \tag{6}$$

where:

$$u_{xi} = \frac{x_{si} - x_{0u}}{R_{0i}}, \quad u_{yi} = \frac{y_{si} - y_{0u}}{R_{0i}}, \quad u_{zi} = \frac{z_{si} - z_{0u}}{R_{0i}} \tag{7}$$

The Matrix $\mathbf{G}$ in Equation (6) is mentioned before the geometric matrix. Equation (6) is over-determined in case of more than four measurements. The solution using the least-square-adjustment is given by:

$$\Delta \hat{\mathbf{X}} = \left(\mathbf{G}^{\mathrm{T}} \mathbf{G} \right)^{-1} \mathbf{G}^{\mathrm{T}} \Delta \boldsymbol{\rho} . \tag{8}$$

Expression $(\mathbf{G}^T\mathbf{G})^{-1}$ is the covariance matrix in the ECEF coordinates system. To compute DOP coefficients in the horizontal coordinates system, $\mathbf{G}$ has to be transformed to the East-North-Up (ENU) coordinates system (see Figure 1). After transformation we obtain:

$$\mathbf{G}_{ENU} = \begin{bmatrix} cos(E_1) \cdot sin(A_1) & cos(E_1) \cdot cos(A_1) & sin(E_1) & 1 \\ cos(E_2) \cdot sin(A_2) & cos(E_2) \cdot cos(A_2) & sin(E_2) & 1 \\ & \vdots & & \\ cos(E_n) \cdot sin(A_n) & cos(E_n) \cdot cos(A_n) & sin(E_n) & 1 \end{bmatrix} \qquad (9)$$

where E_i is the elevation of the i-th satellite and A_i is the azimuth of the i-th satellite.

As a result we obtain:

$$\mathbf{C}_{X\,ENU} = \left(\mathbf{G}_{ENU}^T \mathbf{G}_{ENU}\right)^{-1}$$
$$= \begin{bmatrix} V(E) & cov(E,N) & cov(E,U) & cov(E,c \cdot \delta T) \\ cov(N,E) & V(N) & cov(N,U) & cov(N,c \cdot \delta T) \\ cov(U,E) & cov(U,N) & V(U) & cov(U,c \cdot \delta T) \\ cov(c \cdot \delta T,E) & cov(c \cdot \delta T,N) & cov(c \cdot \delta T,U) & V(c \cdot \delta T) \end{bmatrix} \qquad (10)$$

and DOP can be calculated as follows:

$$\text{global}: \quad GDOP = \sqrt{V(E) + V(N) + V(U) + V(c \cdot \delta T)} \qquad (11)$$

$$\text{position}: \quad PDOP = \sqrt{V(E) + V(N) + V(U)} \qquad (12)$$

$$\text{horizontal}: \quad HDOP = \sqrt{V(E) + V(N)} \qquad (13)$$

$$\text{vertical}: \quad VDOP = \sqrt{V(U)} \qquad (14)$$

$$\text{time}: \quad TDOP = \sqrt{V(c \cdot \delta T)} \qquad (15)$$

Equation (2) shows that a lower value of DOP implies higher accuracy, so the most desired situation (from the autonomous precise navigation point of view) is when DOP values are as low as possible along the whole vehicle route. In order to achieve this, it is essential to compute which satellites will be visible and what values of azimuths and elevations will be like.

3. SATELLITE VISIBILITY. As a part of our research the following methodology of computation of satellites' visibility is proposed. Let us define the following matrices:

Satellites' visibility matrix ($\mathbf{S}_{VS}$):

$$\mathbf{S}_{VS} = \begin{bmatrix} SV_1 & Health_1 & Visible_1 \\ SV_2 & Health_2 & Visible_2 \\ & \vdots & \\ SV_k & Health_k & Visible_k \end{bmatrix} \qquad (16)$$

where SV_i is i-th satellite identification number, $Health_i$ is the i-th satellite health flag (true if satellite status is healthy, false if not), $Visible_i$ is the i-th satellite visibility flag
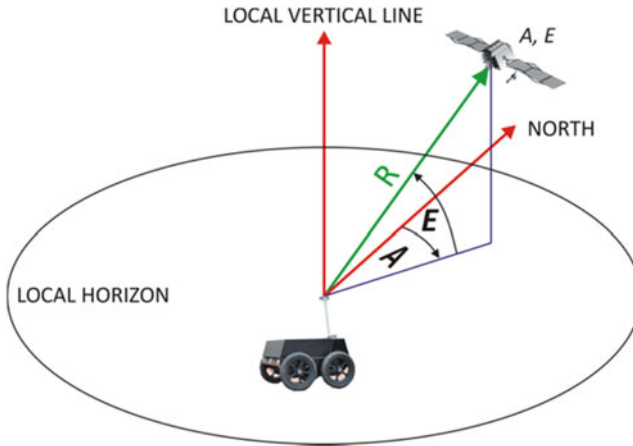
Figure 1. Azimuth and elevation of visible satellite.

(true if satellite is visible, false if not) and k is the total number of satellites in constellations of all analysed systems.

Satellites' azimuths and elevations matrix ($\mathbf{S}_{AE}$):

$$\mathbf{S}_{AE} = \begin{bmatrix} SV_1 & A_{S1} & E_{S1} \\ SV_2 & A_{S2} & E_{S2} \\ & \vdots & \\ SV_k & A_{Sk} & E_{Sk} \end{bmatrix} \tag{17}$$

where A_{Si}, E_{Si} are the azimuth and elevation of i-th satellite (in relation to the vehicle location).

Terrain profile matrix ($\mathbf{T}_{AE}$):

$$\mathbf{T}_{AE} = \begin{bmatrix} A_{T1} & E_{T1} \\ A_{T2} & E_{T2} \\ & \vdots \\ A_{Tl} & E_{Tl} \end{bmatrix} \tag{18}$$

where E_{Ti}, A_{Ti} are the azimuth and maximum elevation of i-th terrain profile (in relation to the vehicle location) and l is the number of analysed terrain profiles.

Now we can claim the following:

$$\mathbf{S}_{VS}(t) = f(\mathbf{S}_{AE}(t), \mathbf{T}_{AE}(t), t) \tag{19}$$

where t is the moment of observation.

The $\mathbf{S}_{AE}$ matrix is dependent on orbit parameters of the individual satellite and the vehicle location:

$$\mathbf{S}_{AE}(t) = f(\mathbf{O}_K(t), \mathbf{V}_L(t), t) \tag{20}$$

where $\mathbf{O}_K(t)$ is the Kepler's orbit parameters matrix for t and $\mathbf{V}_L(t)$ is the vehicle

location matrix for t, wherein:

$$\mathbf{O}_K = \begin{bmatrix} SV_1 & a_1 & e_1 & i_1 & \Omega_1 & \dot{\Omega}_1 & \omega_1 & \mu_{01} & t_{oe1} \\ SV_2 & a_2 & e_2 & i_2 & \Omega_2 & \dot{\Omega}_2 & \omega_2 & \mu_{02} & t_{oe2} \\ & & & & \vdots & & & & \\ SV_j & a_j & e_j & i_j & \Omega_j & \dot{\Omega}_j & \omega_j & \mu_{0j} & t_{oej} \end{bmatrix} \qquad (21)$$

where a_i is the big semi-axis of i-th satellite orbit, e_i is the eccentricity of i-th satellite orbit, i_i is the inclination of i-th satellite orbit, Ω_i is the Right Ascension of the Ascending Node (RAAN) of i-th satellite orbit, $\dot{\Omega}_i$ is the rate of RAAN of i-th satellite orbit, ω_i is the argument of perygeum of i-th satellite orbit, μ_{0i} is the mean anomaly for t_{oe} of i-th satellite orbit, t_{oei} is the time of ephemeris of i-th satellite and

$$\mathbf{V}_L = \begin{bmatrix} \varphi_V & \lambda_V & h_V \end{bmatrix}^T \qquad (22)$$

where $\varphi_V, \lambda_V, h_V$ are the latitude, longitude and ellipsoidal height of the vehicle location. It is assumed that the reference surface for all computations is the WGS-84 ellipsoid.

After azimuths and elevations of all satellites have been computed, matrix ($\mathbf{S}_{AE}$) can be simplified to matrix ($\mathbf{S}'_{AE}$) the elements of which are only (SV_i, A_{Si}, E_{Si}) of satellites above the horizon:

$$\mathbf{S}'_{AE} = \begin{bmatrix} SV_1 & A_{S1} & E_{S1} \\ SV_2 & A_{S2} & E_{S2} \\ & \vdots & \\ SV_{k'} & A_{Sk'} & E_{Sk'} \end{bmatrix} \qquad (23)$$

where k' is the total number of satellites above the horizon.

The $\mathbf{T}_{AE}$ matrix is dependent on terrain shape (approximated by DTM) and the vehicle location:

$$\mathbf{T}_{AE}(t) = f(\mathbf{T}_{DTM}, \mathbf{V}_L(t), t) \qquad (24)$$

From a computational simplicity point of view it is assumed that the DTM model is a rectangular grid (cell dimension: 0·5 m x 0·5 m) where each node has an assigned latitude, longitude and ellipsoidal height (see Figure 2), thus:

$$\mathbf{T}_{DTM} = \begin{bmatrix} \mathbf{T}_{P1,1} & \mathbf{T}_{P1,2} & \cdots & \mathbf{T}_{P1,q} \\ \mathbf{T}_{P2,1} & \mathbf{T}_{P2,2} & \cdots & \mathbf{T}_{P2,q} \\ & \vdots & & \\ \mathbf{T}_{Pp,1} & \mathbf{T}_{Pp,2} & \cdots & \mathbf{T}_{Pp,q} \end{bmatrix} \qquad (25)$$

where:

$$\mathbf{T}_{Pi,j} = \begin{bmatrix} \varphi_{i,j} & \lambda_{i,j} & h_{i,j} \end{bmatrix}^T \qquad (26)$$

and p is the dimension of modelled area in northern direction in metres $\times$ 2 and q is the dimension of modelled area in eastern direction in metres $\times$ 2.

Using DTM it is possible to compute a terrain profile matrix ($\mathbf{T}_{AE}$). To make computations simpler and faster in the proposed method only profiles on azimuths equal to
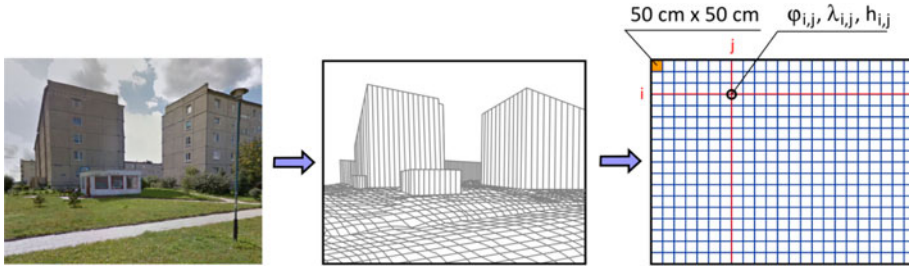
Figure 2. Process of DTM building.

the azimuths of satellites above the horizon are analysed (as shown in Figure 3). Thus the terrain profile matrix ($\mathbf{T}_{AE}$) can be written in the following form:

$$\mathbf{T}_{AE} = \begin{bmatrix} A_{S1} & E_{T1} \\ A_{S2} & E_{T2} \\ & \vdots \\ A_{Sk'} & E_{Tk'} \end{bmatrix} \tag{27}$$

Now visibility of the individual satellite can be defined in the form of the very simple condition:

$$if\ E_{Si}(A_{Si}) > E_{Ti}(A_{Si})\ then\ \ Visible_i = \text{TRUE}\ else\ Visible_i = FALSE \tag{28}$$

The above condition is illustrated in Figure 3.

4. NUMERICAL EXPERIMENT.   As a part of this research, numerical simulation of a small autonomous vehicle mission in the urban environment was performed. Copyrighted software by Aleksander Nowak (the paper's author) was used in the simulations. The software allows loading a DTM and planning the vehicle's route by giving waypoints and the vehicle speed between them. The waypoints can be pointed to directly on the map, input manually via dialogue window or be imported from a text file. The user has the ability to select which navigation satellite systems are used to perform a simulation (GPS, GLONASS, Galileo, BeiDou and additionally SBAS). The current orbit parameters of the systems are imported from almanac files. The user can also choose the start date and time of the simulation. As a result, text files including the satellite visibility and DOP values for points along the route with the desired resolution (standard resolution equals 1 m) are exported by the software. Moreover, the software computes the system availability on the basis of the predefined maximum DOP threshold. The main window of the software is presented in Figure 4.

4.1. *Simulated urban environment.*   The simulated area was within one of the districts in the city of Gdynia, Poland. Its dimensions are 600 m x 600 m. Building density of this place is average and they are mostly five floors high. This is typical for small towns in Poland. The buildings there do not create urban canyons which can be observed in big cities, so at first glance there should not be many problems with GNSS positioning. Three examples of street views typical for this area are shown in Figure 5.
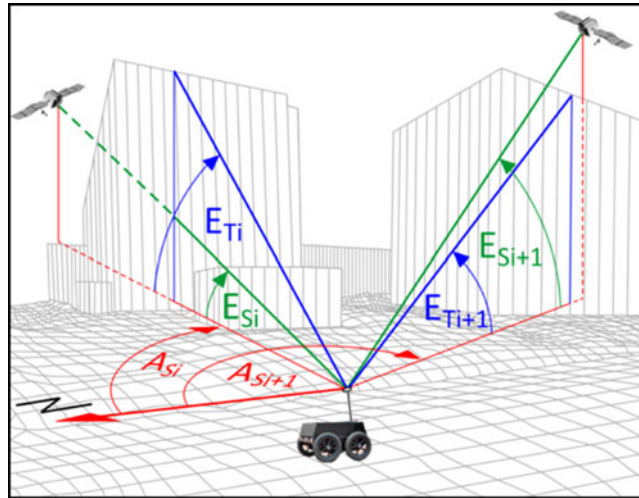
Figure 3. Relation between satellites' elevations (E_{Si}) and maximum elevations of terrain profiles (E_{Ti}).
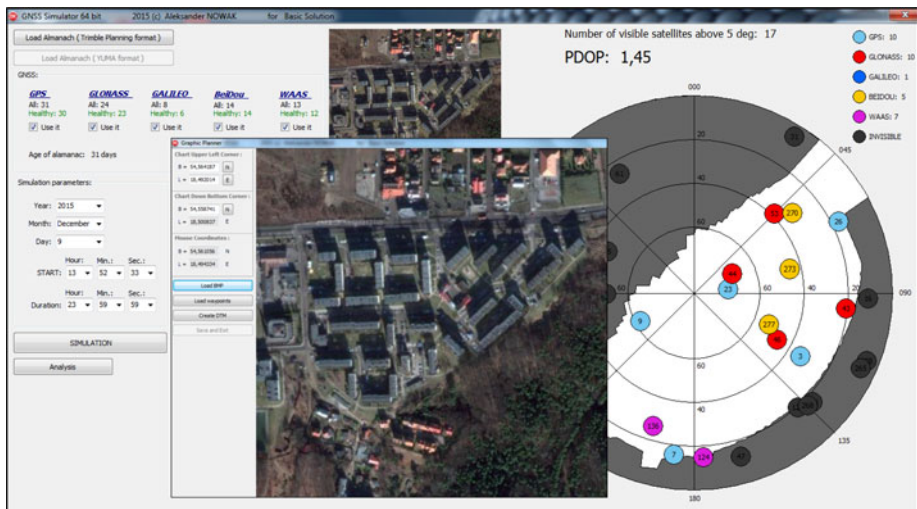

Figure 4. The main window of the built software.

The DTM model of the simulated urban environment was built on the basis of a point cloud from airborne laser scanning. The methodology of DTM building proposed for dynamic GNSS mission planning purposes will be described in another paper, but it should be emphasised here that the required accuracy of DTM is not as high in the case of GNSS mission planning as required in surveying tasks like inventory or cartography. Horizontal and vertical resolution equalling 0·5 m is sufficient. Moreover, it is not necessary to model every detail of terrain and buildings because the most important factor is elevation mask caused by obstructions created by both
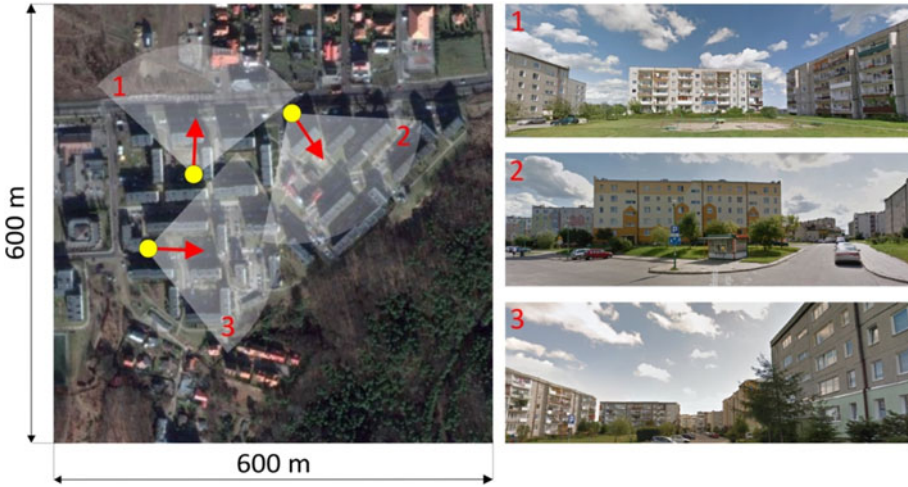
Figure 5. The simulated urban environment (pictures from Google Maps).

man-made and natural features of the urban environment. Therefore, the algorithm of the point clouds to DTM transformation is much simpler.

4.2. *The vehicle and simulated route.* The simulations were performed for a small autonomous Unmanned Ground Vehicle (UGV). Its dimensions are presented in Figure 6. It is assumed that the vehicle goes along the planned route (shown in Figure 6) at constant speed of 1 m/s. The antenna of the GNSS receiver is mounted on the mast 0·8 m above the ground level.

The dead reckoning process for simulation purposes was done on the basis of basic formulae:

$$\begin{aligned} \varphi_V(t + \Delta t) &= \varphi_V(t) + \Delta\varphi_V \\ \lambda_V(t + \Delta t) &= \lambda_V(t) + \Delta\lambda_V \end{aligned} \tag{29}$$

where:

$$\begin{aligned} \Delta\varphi_V &= V_V \cdot \Delta t \cdot cos(H_d) \cdot p_\varphi \\ \Delta\lambda_V &= V_V \cdot \Delta t \cdot sin(H_d) \cdot p_\lambda \end{aligned} \tag{30}$$

and V_V is the vehicle speed in $\left[{}^{m}/_{s}\right]$, H_d is the vehicle heading (course) in [°], Δt is the time interval in [s], p_φ is the transition coefficient from metres to degrees for latitude $\left[{}^{\circ}/_{m}\right]$, p_λ is the transition coefficient from metres to degrees for longitude $\left[{}^{\circ}/_{m}\right]$, wherein:

$$\begin{aligned} p_\varphi &= [1852 \cdot 60]^{-1}, \\ p_\lambda &= \left[1852 \cdot 60 \cdot cos\bigl(\varphi_V(t) + 0 \cdot 5\Delta\varphi_V\bigr)\right]^{-1} \end{aligned} \tag{31}$$

The horizon masks caused by the terrain obstacles for chosen points shown in Figure 6 (points 1, 2, 3) are presented in Figure 7.
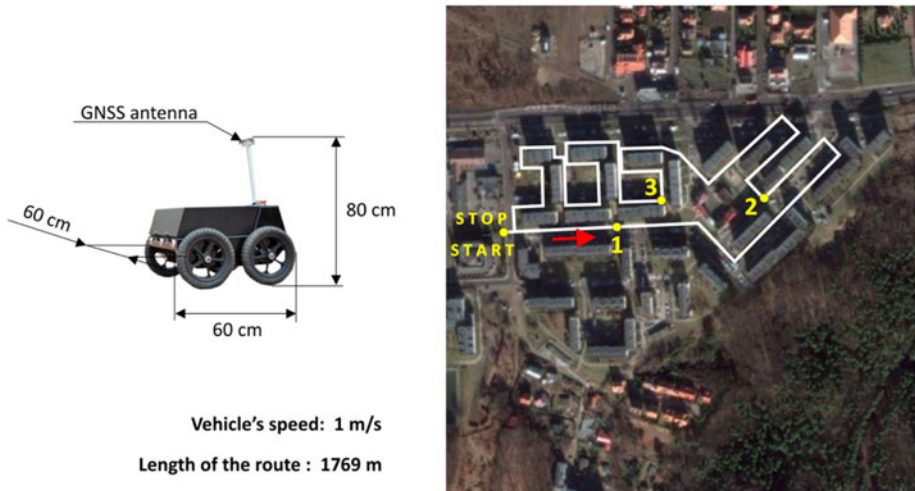
Figure 6. The UGV and its simulated route in the urban environment.
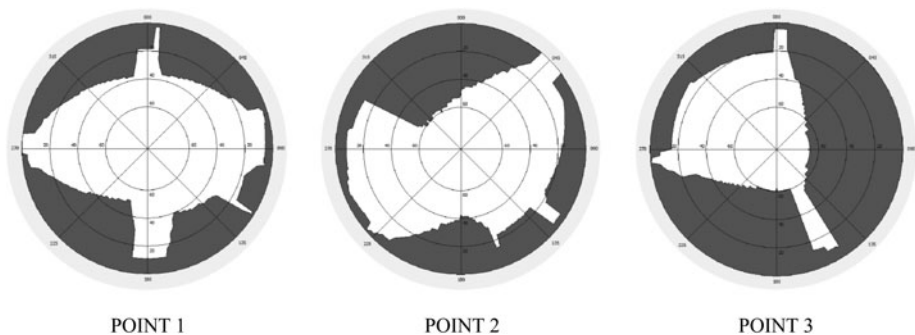

POINT 1 POINT 2 POINT 3

Figure 7. The horizon masks caused by the features of the modeled urban environment for points
1, 2, 3 shown in Figure 3 (print screens from the author's software).

4.3. *The experiment.* During the numerical experiment, the operation of UGV in
the urban environment along the route presented in Figure 6 was simulated. Real and
current almanac data of GPS, GLONASS, Galileo and BeiDou systems were all used
in the simulation. 6 December 2015 was chosen as the day of the simulated UGV op-
eration. To find the best time for the task performance, the availability of a Position
Dilution of Precision (PDOP) value lower than the predetermined maximum threshold
was computed for points along the UGV route with 1 m resolution. Therefore, as a
result of simulation, visibility of satellites and PDOP values were obtained for 1769
points for each passage. The maximum PDOP threshold was set to 5, 4, 3 and 2. The
UGV operation start time was changed from 00:00 to 24:00 with 15 minutes' interval,
therefore 96 passages were analysed for each of the following GNSS configurations:
GPS alone, GPS + GLONASS and GPS + GLONASS + Galilieo + BeiDou. At the
moment of the simulation, individual systems consisted of the following number of
satellites: GPS–31, GLONASS–24, Galileo–8 and BeiDou–14 satellites.

To assess quality of the GNSS positioning during the UGV mission, two states of the system were defined:

1. **Working State** – current PDOP value is not higher than the predetermined maximum PDOP threshold.
2. **Failure State** – current PDOP value is higher than the predetermined maximum PDOP threshold or number of visible satellites is insufficient to fix the position (fewer than four).

Availability of the system is defined as the percentage of the time during which the system was in the working state and this was chosen as a quality measure of the GNSS positioning.

4.4.   *Results of the experiment.*   In order to ensure clarity of the paper and due to the limited volume of the article, only selected and representative results of the numerical experiments are presented.

It is obvious that a multi-system GNSS receiver allows tracking of more satellites, even in urban environments. In Figure 8 it is shown how a significant increase of GNSS positioning quality is achieved when multiple constellations are used. As an example, the number of visible satellites distributed along the route for chosen UGV mission start time is illustrated.

Of course, more observed satellites results in lower DOP values. Figures 9–11 show the DOP distribution along the route for the same UGV mission start time as in the case of Figure 8.

It can be seen that even with a relatively small density of buildings in the modelled urban environment, GPS alone is not sufficient to ensure reliable navigation. A combination of GPS + GLONASS gives much better GNSS performance, but still we have some sections of the vehicle route where PDOP is higher than 6. Additional satellites from Galileo and BeiDou keep PDOP values below level 6. It can be noticed that in the case of GPS alone positioning, a peak on the Horizontal Dilution of Precision (HDOP) chart has appeared and in consequence, it is also visible on the PDOP chart. Buildings cause signals from lower satellites (with low elevations) to be blocked and in consequence visible satellites create unfavourable geometry for the precise fix of horizontal coordinates. Multi-constellation receivers largely compensate this adverse effect.

Figures 12–16 present the GNSS positioning availability as a function of the UGV mission start time, using GNSS systems and predefined maximum PDOP thresholds. Figure 12 presents the positioning availability for any PDOP value, which means that if four satellites were visible, the system was considered to be available. Subsequent figures show the increasing requirements for accuracy (lower admissible maximum PDOP values). The presented graphs clearly show that the GNSS positioning availability for a desired accuracy level depends not only on how many navigation satellites systems are used but also on the UGV mission start time. In other words, there are better and worse time windows to complete the task in the urban environment if the navigation process is based on GNSS. The same simulation results are presented in tabular form in Tables 1–3.

Some types of UGV mission do not require information about height. Due to the fact that the UGV's height above ground level is constant and equals 0, sometimes only horizontal coordinates are taken into account. In such cases, to assess quality
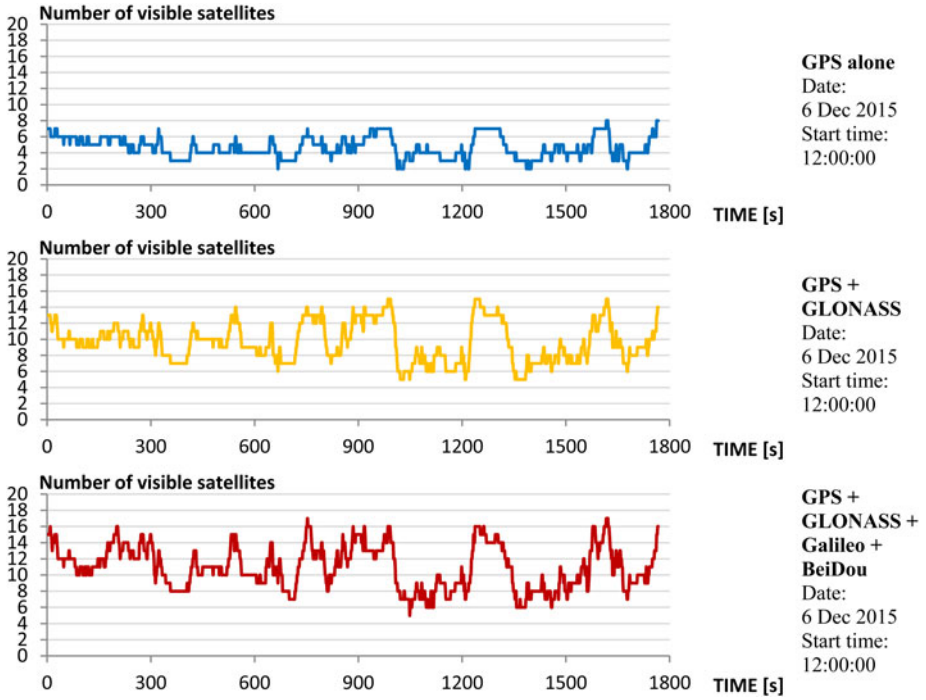
Figure 8. The number of visible satellites distributed along the route for different configurations of the satellite navigation systems.
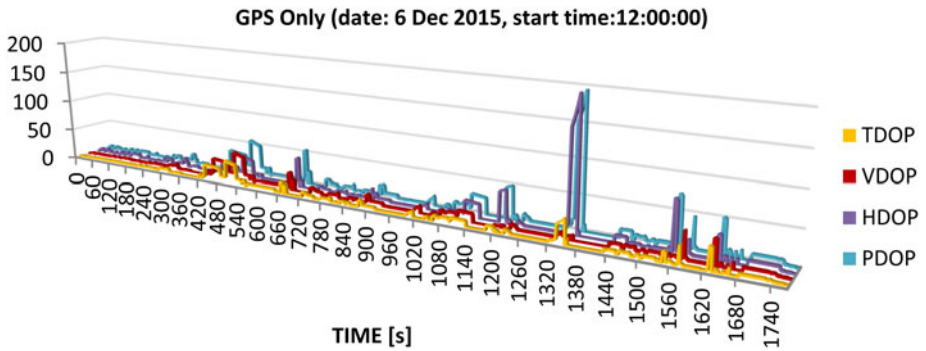

Figure 9. The DOPs distribution along the route for GPS positioning.

of the GNSS positioning during the UGV mission, two states of the system can be defined as:

1. **Working State** – current HDOP value is not higher than the predetermined maximum HDOP threshold.
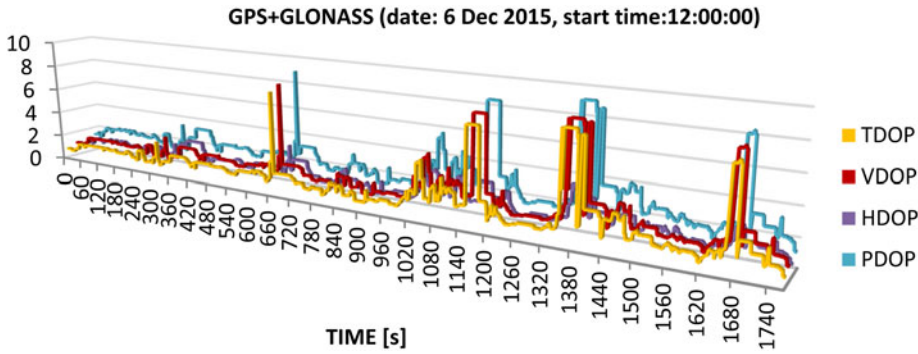
Figure 10. The DOPs distribution along the route for GPS + GLONASS positioning.
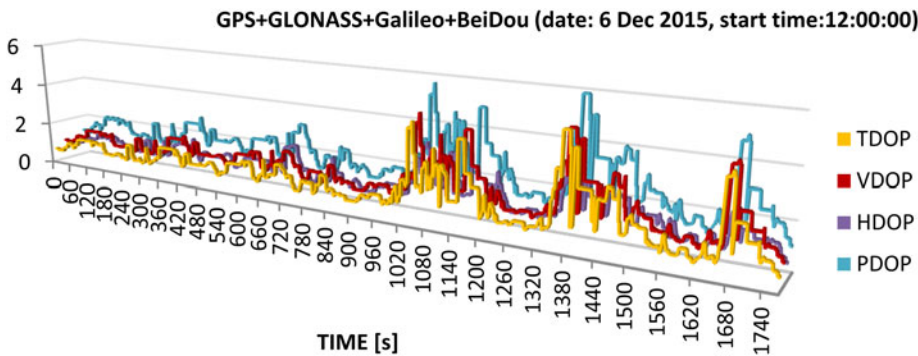
Figure 11. The DOPs distribution along the route for GPS + GLONASS + Galileo + BeiDou positioning.

Figure 12. The GNSS positioning availability for no predefined maximum PDOP threshold, as a function of the UGV mission start time and used GNSS systems (date: 6 Dec 2015).

2. **Failure State** – current HDOP value is higher than the predetermined maximum HDOP threshold or number of visible satellites is insufficient to fix the position (fewer than four).
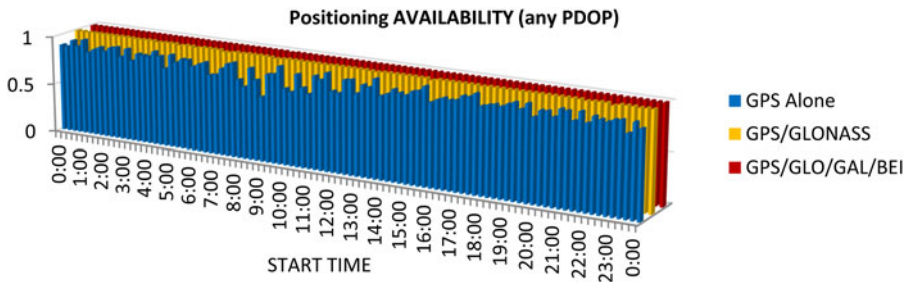
Figure 13. The GNSS positioning availability for predefined maximum PDOP threshold equals 5, as a function of the UGV mission start time and used GNSS systems (date: 6 Dec 2015).

Figure 14. The GNSS positioning availability for predefined maximum PDOP threshold equals 4, as a function of the UGV mission start time and used GNSS systems (date: 6 Dec 2015).

Figure 15. The GNSS positioning availability for predefined maximum PDOP threshold equals 3, as a function of the UGV mission start time and used GNSS systems (date: 6 Dec 2015).

Figures 17–20 and Table 4 present the GNSS availability as a function of the UGV mission start time, used GNSS systems and predefined maximum HDOP thresholds.

In Table 4 the emboldened values represent maximum and minimum GNSS positioning availability for the specified system configuration and predefined HDOP. It can be seen that the differences in the positioning availability are smaller if HDOP
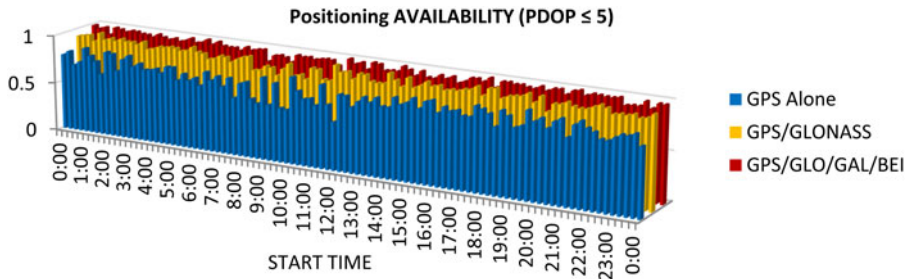
Figure 16. The GNSS positioning availability for predefined maximum PDOP threshold equals 2, as a function of the UGV mission start time and used GNSS systems (date: 6 Dec 2015).
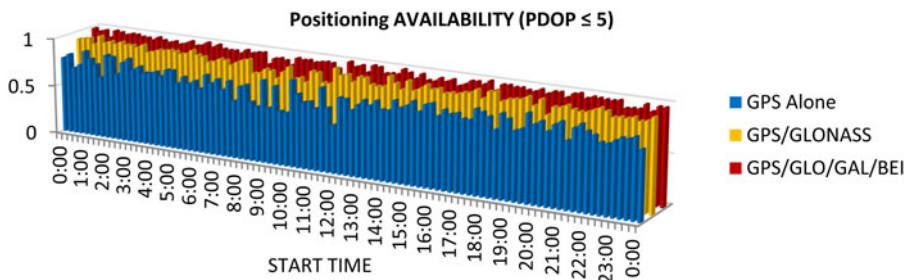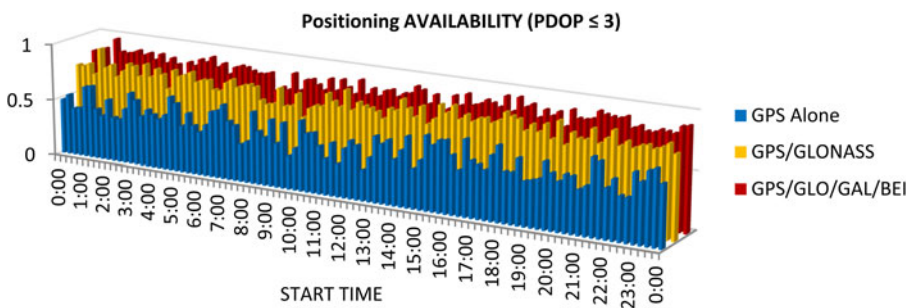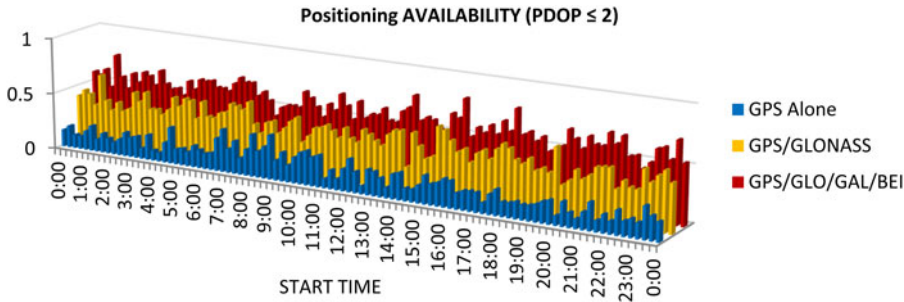
Table 1. The GNSS positioning availability as a function of the UGV mission start time, used GNSS systems and no predefined maximum PDOP threshold (date: 6 Dec 2015).

			GNSS positioning availability [%]							
Start time	GPS	GPS/ GLO	GPS/GLO/ GAL/BEI	Start time	GPS	GPS/ GLO	GPS/GLO/ GAL/BEI	Start time	GPS	GPS/ GLO	GPS/GLO/ GAL/BEI
00:00	90,2	100	100	09:00	65,6	99,0	99,5	17:00	90,1	100	100
01:00	98,3	100	100	10:00	77,4	100	100	18:00	87,9	100	100
02:00	89,2	100	100	11:00	75,2	99,8	100	19:00	93,2	100	100
03:00	95,1	99,8	100	12:00	81,8	100	100	20:00	84,4	100	100
04:00	90,8	99,8	100	13:00	82,8	99,6	100	21:00	95,7	100	100
05:00	95,3	100	100	14:00	84,1	100	100	22:00	85,9	100	100
06:00	86,4	100	100	15:00	87,9	99,8	99,9	23:00	92,6	100	100
07:00	81,6	98,8	100	16:00	84,5	100	100	24:00	87,9	100	100
08:00	79,6	100	100								

is taken into account instead of PDOP but are still significant in the case of GPS-only positioning (from 31·9% to 41,1%). Moreover, the differences grow with the increase of the accuracy requirements (with one exception in the case of GPS-only positioning). If maximum HDOP threshold is set at 2, the difference reaches 23·3% even if a multi-constellation receiver is used. It proves again that dynamic GNSS mission planning is necessary in order to ensure reliable navigation for the UGV even if only the horizontal accuracy is taken into account. In order to show how GNSS positioning availability increases when only horizontal coordinates are taken into consideration, differences between GNSS availabilities for predefined maximum HDOP and PDOP thresholds are shown in Figures 21–24.

Looking at Figures 21–24, it can be seen that the difference between positioning availability in the horizontal plane and in three-dimensional space increases with the increase of the precision requirements. It is almost negligible if HDOP and PDOP thresholds are set at 5 and quite significant when the thresholds are set at 2. This means that precise navigation in three dimensions using GNSS requires more careful planning. It is worth remembering that simulations were performed for an area with average building density, where building height is only four or five floors.

Table 2. The GNSS positioning availability as a function of the UGV mission start time, used GNSS systems and predefined maximum PDOP threshold (date: 6 Dec 2015).

						GNSS availability for predefined PDOP thresholds [%]						
Constellation		GPS	GPS/GLO	GPS/GLO/ GAL/BEI	GPS	GPS/GLO	GPS/GLO/ GAL/BEI	GPS	GPS/GLO	GPS/GLO/ GAL/BEI	GPS	GPS/GLO	GPS/GLO/ GAL/BEI
PDOP thresholds			5			4			3			2	
The UGV mission start time	00:00	78,6	92,7	99,2	69,5	91,6	93,8	48,9	75,4	83,6	15,2	41,5	58,5
	01:00	**88,3**	**99,1**	**99,3**	78,4	**97,8**	**98,3**	63,0	**92,6**	**96,7**	17,1	**62,9**	**76,3**
	02:00	87,4	95,9	98,1	**79,6**	89,3	96,8	54,2	75,2	88,9	13,4	33,1	54,1
	03:00	86,5	96,0	98,3	79,0	90,7	94,3	63,3	84,1	88,4	17,4	53,1	67,8
	04:00	75,1	93,1	94,2	62,9	87,1	89,0	46,9	65,1	72,2	9,2	40,5	48,3
	05:00	81,0	93,3	96,4	72,9	90,5	93,0	60,0	82,9	86,6	13,4	51,8	64,0
	06:00	73,5	87,5	95,7	63,4	84,1	89,6	37,7	70,2	78,9	16,1	39,3	58,1
	07:00	78,5	87,7	97,5	75,2	82,8	92,8	65,0	75,3	84,7	37,6	53,1	68,6
	08:00	74,5	82,8	**86,1**	56,2	75,7	**77,7**	**35,8**	67,0	**70,4**	23,1	32,0	**41,9**
	09:00	84,2	**80,7**	88,5	79,1	**74,9**	80,2	57,9	**64,7**	73,4	**38,9**	39,8	52,6
	10:00	54,6	84,7	94,3	**38,4**	80,0	89,1	36,4	65,8	76,5	22,7	36,1	47,2
	11:00	69,6	83,0	91,2	65,5	81,0	88,0	41,7	75,1	81,9	27,9	43,8	60,1
	12:00	**49,5**	94,4	98,0	46,8	93,0	94,3	42,7	77,3	83,9	19,4	36,8	55,9
	13:00	73,4	87,9	93,0	68,1	80,4	90,5	38,2	66,2	79,7	22,3	37,3	52,1
	14:00	72,3	92,6	97,0	61,3	86,1	95,9	40,2	78,2	88,6	21,7	**22,2**	56,7
	15:00	79,6	90,8	91,7	70,2	85,2	86,1	42,6	72,3	75,4	15,6	34,5	47,6
	16:00	85,6	89,3	90,5	76,6	85,3	88,4	62,9	75,1	81,8	24,7	41,8	49,2
	17:00	79,1	93,6	95,4	70,8	89,4	92,9	49,2	79,3	83,1	17,6	46,7	54,4
	18:00	84,1	98,1	98,2	78,1	95,2	96,0	**65,2**	84,1	86,2	22,6	51,6	57,4
	19:00	80,9	94,0	95,3	68,1	88,0	91,8	39,0	74,0	81,9	13,2	36,0	46,4
	20:00	79,2	82,4	98,1	62,9	78,4	88,4	49,2	66,3	82,9	20,5	27,3	60,5
	21:00	85,5	91,1	95,5	75,9	88,7	92,5	38,9	83,1	89,2	**8,6**	38,9	57,7
	22:00	80,2	96,1	96,9	59,9	90,4	93,4	43,9	72,1	81,2	15,9	30,9	52,3
	23:00	74,6	89,7	92,3	71,3	85,9	88,6	60,2	76,1	82,9	16,0	51,3	61,9
	24:00	70,4	94,3	97,0	65,9	88,9	95,2	54,2	72,2	89,3	17,1	42,9	53,3

Table 3. Maximum and minimum GNSS availability as a function of used GNSS systems and predefined maximum PDOP threshold (date: Dec. 6, 2015).

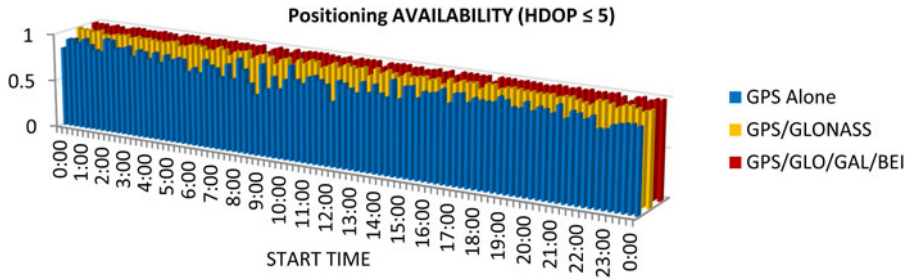| Constellation	Maximum and minimum GNSS availability for predefined PDOP thresholds [%]											
	GPS	GPS/GLO	GPS/GLO/ GAL/BEI	GPS	GPS/GLO	GPS/GLO/ GAL/BEI	GPS	GPS/GLO	GPS/GLO/ GAL/BEI	GPS	GPS/GLO	GPS/GLO/ GAL/BEI
PDOP thresholds		5			4			3			2	
Maximum availability	88,3	99,1	93,3	79,6	97,8	98,3	65,2	92,6	97,7	38,9	62,9	76,3
(start time)	01:00	01:00	01:00	02:00	01:00	01:00	18:00	01:00	01:00	09:00	01:00	01:00
Minimum availability	49,5	80,7	86,1	38,4	74,9	77,7	38,8	64,7	70,4	8,6	22,2	41,9
(start time)	12:00	09:00	08:00	10:00	09:00	08:00	08:00	09:00	08:00	21:00	14:00	08:00
Difference	**38,8**	**18,4**	**7,2**	**41,2**	**22,9**	**20,6**	**26,4**	**27,9**	**27,3**	**30,3**	**40,7**	**34,4**

Figure 17. The GNSS positioning availability for predefined maximum HDOP threshold equals 5, as a function of the UGV mission start time and used GNSS systems (date: 6 Dec 2015).

Figure 18. The GNSS positioning availability for predefined maximum HDOP threshold equals 4, as a function of the UGV mission start time and used GNSS systems (date: 6 Dec 2015)

Figure 19. The GNSS positioning availability for predefined maximum HDOP threshold equals 3, as a function of the UGV mission start time and used GNSS systems (date: 6 Dec 2015).
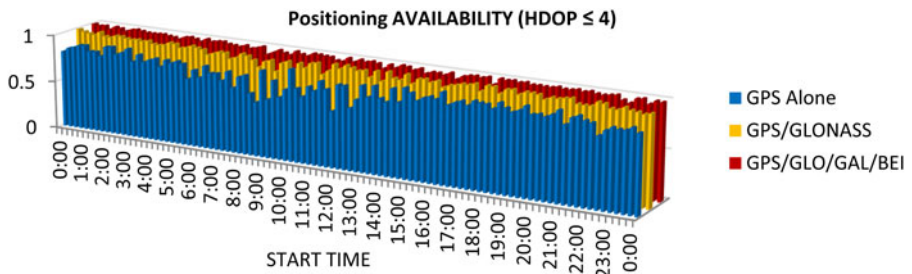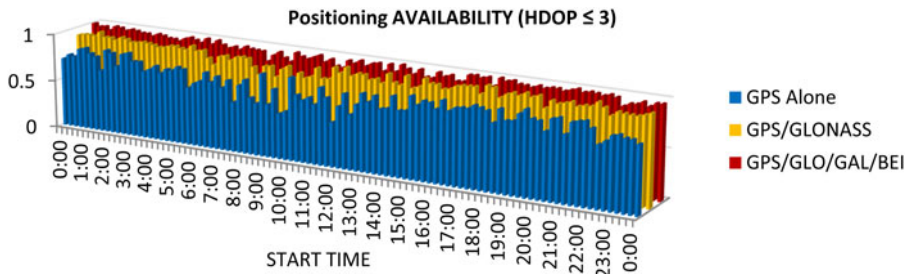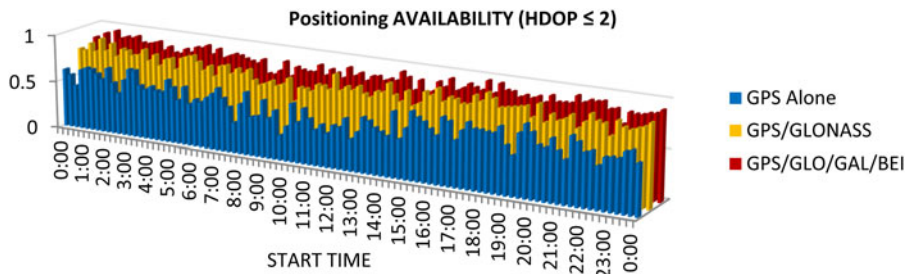

Figure 20. The GNSS positioning availability for predefined maximum HDOP threshold equals 2, as a function of the UGV mission start time and used GNSS systems (date: 6 Dec 2015).

Table 4. The GNSS positioning availability as a function of the UGV mission start time, used GNSS systems and predefined maximum HDOP threshold (date: 6 Dec 2015).

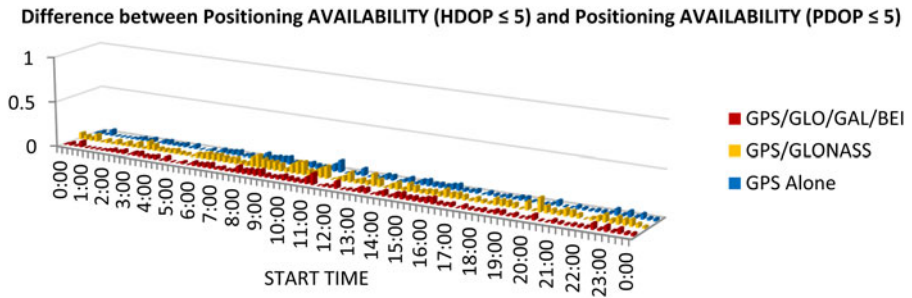| Constellation		GNSS availability for predefined PDOP thresholds [%]										
		GPS	GPS/GLO	GPS/GLO/ GAL/BEI	GPS	GPS/GLO	GPS/GLO/ GAL/BEI	GPS	GPS/GLO	GPS/GLO/ GAL/BEI	GPS	GPS/GLO	GPS/GLO/ GAL/BEI
HDOP thresholds			5			4			3			2	
The UGV mission start time	00:00	83,9	99,9	**100,0**	81,2	99,6	**100,0**	72,6	92,5	**99,8**	61,8	78,6	85,7
	01:00	96,5	**100,0**	**100,0**	90,5	99,5	99,8	86,8	**98,7**	99,2	66,3	**92,4**	**95,7**
	02:00	**99,5**	98,0	99,9	92,2	97,9	99,9	87,7	95,9	97,5	69,3	84,4	92,7
	03:00	94,7	97,5	98,7	93,2	96,1	98,3	**87,9**	94,2	97,2	**71,4**	87,0	90,2
	04:00	84,8	96,4	96,8	84,7	95,3	95,9	73,9	91,9	93,0	56,4	79,7	80,2
	05:00	86,8	95,8	96,8	84,7	95,7	96,7	76,1	92,5	94,4	59,0	86,2	89,5
	06:00	81,9	94,7	**100,0**	80,7	91,4	99,6	65,7	86,9	95,3	49,6	79,3	82,2
	07:00	84,7	92,8	99,4	80,5	90,3	98,7	76,3	88,0	96,5	65,0	74,6	84,7
	08:00	98,3	93,0	**93,6**	80,3	92,3	**92,5**	70,7	84,2	**84,4**	52,1	71,3	**72,4**
	09:00	95,8	**90,1**	95,9	90,3	**83,7**	95,3	86,2	**77,3**	87,2	59,5	**68,6**	72,9
	10:00	83,1	98,1	**100,0**	74,1	95,5	99,8	50,6	84,7	95,3	**35,8**	70,4	80,6
	11:00	89,1	93,2	98,8	80,6	87,3	96,1	68,5	82,1	89,4	47,6	75,6	83,0
	12:00	**67,6**	**100,0**	**100,0**	**59,0**	**100,0**	**100,0**	**46,8**	97,1	98,1	44,3	78,3	86,3
	13:00	79,7	92,0	94,7	74,3	91,3	94,4	68,6	87,8	90,8	41,1	70,9	81,8
	14:00	83,0	97,3	**100,0**	79,3	93,6	99,3	67,7	88,4	96,4	45,3	76,7	88,7
	15:00	93,6	97,4	98,4	**93,5**	96,4	97,3	69,6	87,7	90,4	52,8	71,8	77,9
	16:00	90,4	93,5	96,2	88,1	91,4	93,6	81,3	88,7	90,8	55,7	76,8	81,9
	17:00	93,7	98,6	99,4	85,8	97,4	98,6	79,5	95,3	97,5	48,2	77,9	85,8
	18:00	90,5	**100,0**	**100,0**	89,1	99,0	99,3	83,5	97,5	97,6	62,2	87,3	89,3
	19:00	94,3	98,8	99,6	87,7	94,7	98,3	74,2	92,9	94,8	50,9	82,8	84,9
	20:00	87,2	97,7	**100,0**	84,9	93,4	99,6	79,9	84,1	97,2	67,6	70,7	84,6
	21:00	97,2	98,5	99,0	92,7	98,2	98,5	84,5	93,8	96,9	53,9	82,0	87,7
	22:00	86,7	98,7	99,2	86,3	98,1	98,6	85,2	97,2	98,1	56,2	79,7	84,8
	23:00	84,4	97,5	98,6	83,3	96,4	98,4	74,6	89,5	92,5	55,2	77,3	83,6
	24:00	86,8	96,4	99,8	81,8	94,1	98,6	70,1	93,6	96,1	53,4	85,2	91,1

Figure 21. The difference between GNSS positioning availability for predefined maximum HDOP and PDOP thresholds equal 5 as a function of the UGV mission start time and used GNSS systems (date: 6 Dec 2015).
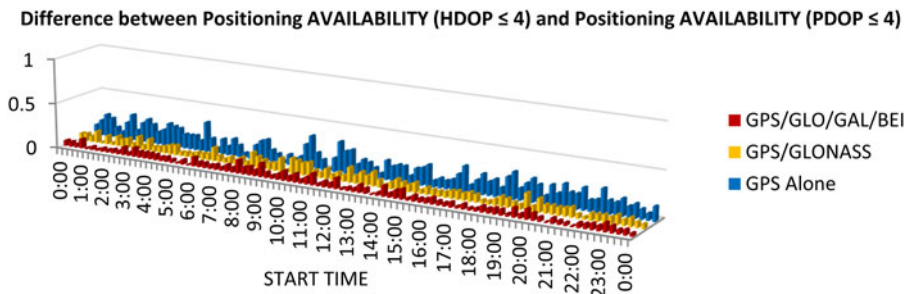

Figure 22. The difference between GNSS positioning availability for predefined maximum HDOP and PDOP thresholds equal 4 as a function of the UGV mission start time and used GNSS systems (date: 6 Dec 2015).
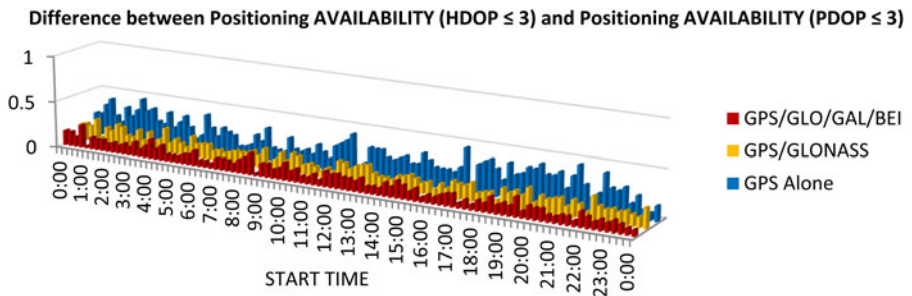

Figure 23. The difference between GNSS positioning availability for predefined maximum HDOP and PDOP thresholds equal 3 as a function of the UGV mission start time and used GNSS systems (date: 6 Dec 2015).

If the building density is greater and buildings higher dynamic GNSS mission planning will play a key role.

Usually, Vertical and Time DOP (VDOP and TDOP) coefficients are not taken into account as separate quality factors of GNSS positioning, as far as we talk about
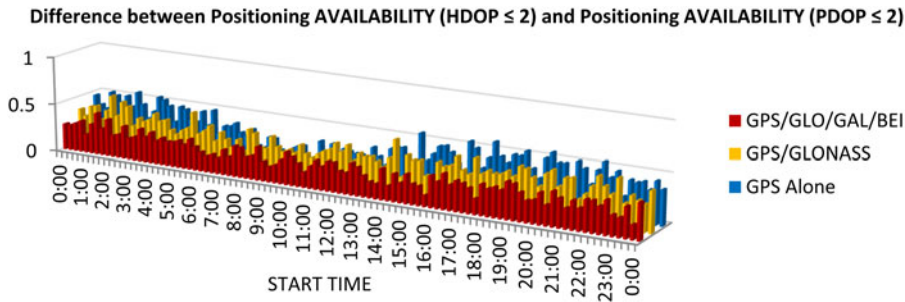
Figure 24. The difference between GNSS positioning availability for predefined maximum HDOP and PDOP thresholds equal 2 as a function of the UGV mission start time and used GNSS systems (date: 6 Dec 2015).

autonomous navigation of ground vehicles. Therefore, and due to the limited volume of the paper, a similar analysis for VDOP and TDOP as for PDOP and HDOP are not presented.

4. CONCLUDING REMARKS. The numerical experiments in this paper have shown that the combined use of the two full operational global navigation satellite systems (GPS and GLONASS) along with additional satellites of the systems under construction, provides a much better quality of service in an urban area than GPS alone. But cities are still challenging environments for positioning using GNSS. Moreover, the availability and accuracy of the GNSS positioning are decreased even in areas with average building density, where building height is only four or five floors. Furthermore, the GNSS positioning availability with desired accuracy differs significantly depending on the UGV mission start time. For the presented simulated route of a small UGV, differences reached up to 40%. In order to meet high positioning accuracy requirements, the PDOP or HDOP values have to be low. In Tables 2 and 4 it can be seen that if predefined maximum PDOP or HDOP value equals 2, in spite of a multi-constellation receiver being used; the positioning availability can differ significantly depending on UGV mission start time. This is related to the constantly changing geometry of visible satellites. At certain times of the day, the geometrical arrangement of GNSS constellations allows observation of more satellites among the buildings. This demonstrates that dynamic GNSS mission planning is necessary to provide reliable and precise positioning data for navigation.

Further research will be focused on the problem of the navigation process optimisation in high building urban environments. The UGV mission start time as presented in this paper will not be the only factor taken into consideration as an element of the optimisation. UGV speed including stops will also be taken into account.

REFERENCES

Angrisano, A., Gaglione, S., Gioia, C. (2013). Performance assessment of GPS/GLONASS single point positioning in an urban environment. *Acta Geodaetica et Geophysica*, **48**(2), 149–161

Asavasuthirakul, D., Karimi, H.A. (2013). Integrated GNSS QoS prediction for navigation services. *Proceedings of the Sixth ACM SIGSPATIAL International Workshop on Computational Transportation Science*, Orlando, FL, 73–78.

Bradbury, J., Ziebart, M., Cross, P.A. (2007). Code Multipath Modelling in the Urban Environment Using Large Virtual Reality City Models: Determining the Local Environment. *The Journal of Navigation*, **60**, 95–105.

Dah, J.J, Chi-Fan, Y., Chih-Hsun, C., Ting-Yu, L. (2013). Performance enhancement for ultra-tight GPS/ INS integration using a fuzzy adaptive strong tracking unscented Kalman filter. *Nonlinerar Dynamics*, **73**(1), 377–395

Dong, G., Yang, Z., Song, L., Ye, K., Li, G., (2015). The Global Shortest Path Visualization Approach with Obstructions, *Journal of Robotics and Mechatronics*, **27**(5), 579–585

Gibbons, G., Divis, D.A., Gutierrez, P. (2013). The GNSS quartet: Harmonizing GPS, GLONASS, BeiDou and Galileo. *Inside GNSS*, **8**(1), 38–44.

Godha, S., Cannon, M.E. (2007), GPS/MEMS INS integrated system for navigation in urban areas. *GPS Solutions*, **11**(3), 193–203

Grejner-Brzezinska, D.A., Yi, Y., Toth, C.K. (2001). Bridging GPS Gaps in Urban Canyons: The Benefits of ZUPTs. *NAVIGATION. Journal of the Institute of Navigation*, **48**(4), 216,226.

Janowski, A., Nowak, A., Przyborski, M., Szulwic, J. (2014). Mobile indicators in GIS and GPS positioning accuracy in cities. *Rough Sets and Intelligent Systems Paradigms, Lecture Notes in Computer Science*, **8537**, 309–318.

Karimi, H.A., Asavasuthirakul, D. (2014). A Novel Optimal Routing for Navigation Systems/Services Based on Global Navigation Satellite System Quality of Service. *Journal of Intelligent Transportation Systems: Technology, Planning, and Operations*, **18**, 286–298.

Kitamura, M., Yasuoka, Y., Suzuki, T., Amano, Y., Hashizume, T. (2013). Path Planning for Autonomous Vehicles Using QZSS and Satellite Visibility Map. *Journal of Robotics and Mechatronics*, **25**(2), 400–407.

Kitamura, M., Suzuki, T., Amano, Y., Hashizume, T. (2011). Improvement of GPS and GLONASS Positioning Accuracy by Multipath Mitigation Using Omni Directional Infrared Camera. *Journal of Robotics and Mechatronics*, **23**(6), 1125–1131.

Li, J., Taylor, G., Kidner, D., Ware, M. (2006). Prediction of GPS multipath effect using LiDAR digital surface models and building footprints. *Lecture Notes in Computer Science*, **4295**, 42–53.

Nowak, A. (2015). The Proposal to "Snapshot" RAIM method for GNSS vessel receivers working in poor space segment geometry, *Polish Maritime Research*, **4**(88), 3–8

Nowak, A., Specht, C. (2008). Computer Simulator of GNSS Measurements. *Annual of Navigation*, *The Journal of Polish Navigational Forum*, **12**, 65–74.

Parkinson, B.W., Spilker, J.J. (1996), *Global Positioning System: Theory and Applications*, Volume II, AIAA, Progress in Astronautics and Aeronautics.

Radisic, T., Novak, D., Bucak, T. (2010). The Effect of Terrain Mask on RAIM Availability. *The Journal of Navigation*, **63**, 105–117.

Roongpiboonsopit, D., Karimi, H.A. (2012). Integrated global navigation satellite system (iGNSS) QoS prediction. *Photogrammetric Engineering & Remote Sensing*, **78**(2), 139–149.

Soloviev, A., Van Graas, F. (2009). Use of Deeply Integrated GPS/INS Architecture and Laser Scanners for the Identification of Multipath Reflections in Urban Environments. *IEEE Journal of Selected Topics in Signal Processing*, **3**(5), 786–797

Suh, Y., Shibasaki, R. (2007). Evaluation of satellite-based navigation services in complex urban environments using a threedimensional GIS. *IEICE Transactions on Communications*, **90**(7), 1816–1825.

Taylor, G., Li, J., Kidner, D., Brunsdon, C., Ware, M. (2007). Modelling and prediction of GPS availability with digital photogrammetry and LiDAR. *International Journal of Geographical Information Science*, **21**(1), 1–20.